Heliyon 10 (2024) e34499

Contents lists available at ScienceDirect

Heliyon

journal homepage: www.cell.com/heliyon

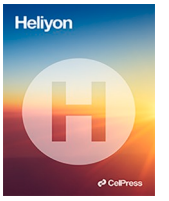

Research article

Investigation on synthesized sulfonamide Schiff base with DFT approaches and in silico pharmacokinetic studies: Topological, NBO, and NLO analyses

Md Minhazul Abedin [a], Tarun Kumar Pal [a,*], Md Chanmiya Sheikh [b], Md Ashraful Alam [a]

[a] Department of Chemistry, Rajshahi University of Engineering & Technology, 6204, Bangladesh
[b] Department of Chemistry, University of Rajshahi, 6205, Bangladesh

ARTICLE INFO

Keywords:
DFT
Topological study
ADMET drug-likeness
Molecular docking
NLO

ABSTRACT

The sulfonamide Schiff base ($C_{16}H_{14}N_4O_3S$) was successfully synthesized and experimentally ascertained. The main purpose of this research is to investigate the geometry of the aforesaid molecule using both experimental and density functional theory (DFT) techniques and determine its drug likeness characteristics, docking ability as an insulysin inhibitor, and its NLO property. For the computational investigations the DFT approaches were utilized at the B3LYP level with the 6-311G+(d,p) basic set. The experimental results of the compound (such as FT-IR, UV–Vis, and ^{1}H NMR) were compared with simulated data. The both results were well and consistent with previously related published data. The obtained spectral results confirm the formation of the Schiff base compound. Both π—π* and n—π* interactions were found in experimental and computational UV–Vis spectra, as well as in the natural bond orbital (NBO) study. The molecular, electronic, covalent, and non-covalent interactions were analyzed using DFT studies. Both experimental and simulation results revealed that the compound is successfully formed and relatively stable. The compound with a lower band gap showed high chemical reactivity. The medicinal characteristics of the compound were evaluated using in silico medicinal methods. The investigated compound was also followed Pfizer, Golden Triangle, GSK as well as Lipinski's rules. Therefore, the compound has more favorable absorption, distribution, metabolism, excretion, and toxicity (ADMET) profile and it can be used as non-toxic oral drug candidate. The compound was exhibited good insulysin inhibitory activity and it has almost eighteen times higher non-linear optical properties than urea and three times higher than potassium dihydrogen phosphate (KDP).

1. Introduction

Azomethine linkage containing organic molecule is known as Schiff base. It is created by German chemist Hugo Schiff [1,2]. It is easily resulted by the condensation reaction between a carbonyl compound and a primary amine. The Schiff bases also contain various electron supplier atoms such as oxygen, sulfur, and nitrogen. These are prominent chelating ligand and extensively employed in coordination chemistry. Moreover, these Schiff base compounds are very stable and their synthetic approach is fairly simple.

* Corresponding author.
E-mail addresses: tkpchem@gmail.com, tkpal@chem.ruet.ac.bd (T.K. Pal).

https://doi.org/10.1016/j.heliyon.2024.e34499
Received 13 May 2024; Received in revised form 8 July 2024; Accepted 10 July 2024
Available online 11 July 2024

Therefore, Schiff base synthesis and complexation have been extensively researched in advanced undergraduate programs [3,4]. Furthermore, sulfonamide Schiff bases contain both azomethine and sulfonamide (–SO_2–NH-) functional groups, which are responsible for their biological activity [5,6]. Therefore, sulfonamide compounds play a crucial role in pharmacological activity. Sulfonamide compounds impede the metabolic pathway of the enzyme dihydropteroate synthase (DHPS) and serve as a bactericidal agent. Sulfamethoxazole comprises a sulfonamide group, which structurally resembles para-amino benzoic acid. Its mechanism involves inhibiting the production of dihydropteroic acid by blocking DHPS, thereby impeding bacterial growth [7,8]. Besides, its primary utilization is for the treatment of urinary tract and gastro intestinal infections [9,10]. Sulfonamide Schiff bases can easily form stable complexes with various transition metal ions [8,11] due to their chelating ability. The producing transition metal complexes have become significantly important in the fields of material science and bioorganic chemistry [9,12]. Metal complexes of sulfonamide Schiff bases have also been shown various biological activities [13,14]. Sulfonamide compounds find to have broad applications as antibacterial, antifungal, anticancer, anti-inflammatory, antiviral agents and also HIV protease inhibitors [2,4,6,9]. Recently, computational methods are becoming reliable and convenient since the experimental results can be hypothesized before performing chemical analysis in lab and both results are fairly consistent [15]. To the best of our knowledge, there is no information available on the quantum chemical calculation (DFT) and comparative studies between experimental and computational analyses of the mentioned compound. Therefore, we synthesized it through a straightforward condensation reaction using sulfamethoxazole and pyridine-2-carbaldehyde, and characterized it using experimental techniques alongside extensive DFT studies. This study also includes a comparative assessment of experimental and computational approaches. Furthermore, we presented findings on frontier molecular orbitals, molecular electrostatic potential (MEP), ADMET, drug likeness, in silico molecular docking, electron localization function (ELF)/localized orbital locator (LOL), reduced density gradient (RDG), natural bond orbital, and non-linear optical (NLO) studies of the specified compound.

2. Experimental approaches

2.1. Materials and methods

The selected aromatic aldehyde and primary amine were bought from Sigma-Aldrich and all the required solvents were acquired from a reliable chemical supplier. The melting point of the final product was assessed through the open capillary technique. The electronic spectra, FT-IR, and melting point of the synthesized product were evaluated through PG Instruments CT60 in dimethylsulfoxide (DMSO), SHIMADZU IR Affinity-1S, and capillary melting point apparatus (COLE-PARMER LTD. STONE, ST150SA, UK), respectively at the departmental laboratory, Department of Chemistry, Rajshahi University of Engineering & Technology, Bangladesh. The ^{1}H NMR spectral analysis of the final purified product was performed in DMSO with the help of the JEOL JNM-ECZ400S a sophisticated 400 MHz ^{1}H NMR spectrometer from Okayama University of Science, Japan. Non-covalent and covalent interactions within the studied molecule were conducted using the Multiwfn 3.8, VMD, Gaussian, irfanView, and gnuplot softwares [16–19]. NBO, and NLO studies were performed using Gaussian programs following the DFT method with same level of theory. The molecular docking analysis was carried out against two receptor proteins (PDB ID: 3E4A) and (PDB ID: 3OFI). ML345 compound (PubChem-CID: 57390068) and 6bK were utilized as standard inhibitors.

2.2. Theoretical approaches

The computational evaluations were performed under the DFT method with basis set of B3LYP/6-311G+(d,p) using Gaussian 09W software and GaussView 6.0.16 visualizer program [16,17]. The optimized molecular state, molecular electrostatic potential,

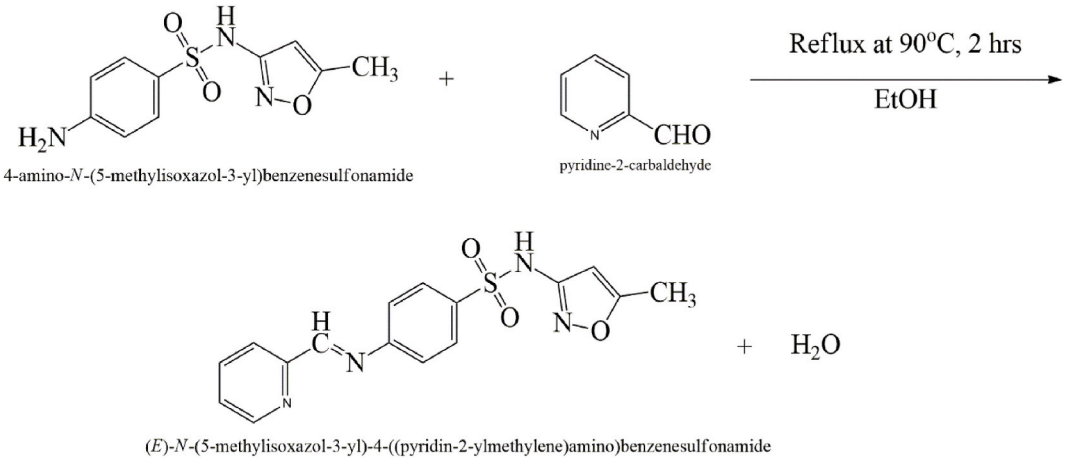

Scheme 1. Reaction scheme for the formation of the studied compound.

HOMO-LUMO, NBO, NLO, and computational spectral data were generated using the Gaussian software. The topological parameters (ELF/LOL and RDG) were also performed using Gaussian, Multiwfn 3.8, and VMD softwares.

2.3. Synthesis of (E)-N-(5-methylisoxazol-3-yl)-4-((pyridin-2-ylmethylene)amino)benzenesulfonamide compound

Equimolar amount of pyridine-2-carbaldehyde (1.07 g, 0.01 mol) and sulfamethoxazole (2.53 g, 0.01 mol) were dissolved in ethanol separately. Then the homogeneous ethanolic mixture of pyridine-2-carbaldehyde was added to the ethanolic mixture of sulfamethoxazole. The resulting mixture was refluxed for 2 h at 90 °C. Finally, yellowish-orange colored precipitates were settled down (Scheme 1). After filtration, the crude precipitates were cleansed with hot ethanol. Then the resulting product was dried. The final product was successfully crystalized with 65 % yield. The melting point of the pure product was 285 °C.

3. Results and discussion

3.1. FT-IR spectra

The vibrational spectrum exhibited the IR absorption frequencies of the bonds present in the studied compound. The compound showed a sharp band at 1605 cm^{-1} due to the stretching vibration of azomethine linkage (-CH═N-) [7,20,21]. The stretching mode of vibration of N–H group was found at 3225 cm^{-1} [7,22]. Theoretically, CH═N and N–H groups were observed at 1637 and 3413 cm^{-1}, respectively (Table 1). The corresponding asymmetric and symmetric modes of the SO_2 group were experimentally found at 1304 cm^{-1} and 1112 cm^{-1} [23,24] whereas they were computationally obtained at 1269 cm^{-1} and 1081 cm^{-1}, respectively. The spectrum exhibited two absorption bands at 1240 cm^{-1} [7,25] for the C–O group and 860 cm^{-1} [20] for the S–N group of the sulfonamide moiety. Theoretically, C–O and S–N bands were appeared at 1250, and 896 $\mathbf{cm^{-1}}$, respectively. The results from the quantum chemical calculation indicated a slight shift toward higher frequencies compared to the experimental data. This shifting is observed because the quantum chemical computations were carried out in the gas phase, whereas the experimental calculations were performed in the solid phase.

3.2. UV–vis spectra

UV–Visible spectral result gives the information about the electronic transition of the compound [26]. In the UV–Vis spectral analysis, π—π* transitions correspond to the electrons present in the conjugated system whereas n—π* corresponds to the non-boding electrons in atoms. The electronic spectrum of the discussed molecule was observed using a 200–800 nm spectrophotometer. Two electronic bands were found in the experimental spectrum at 228 and 256 nm that were corresponded to π—π* transition of the phenyl rings and azomethine linkage [15,20]. On the other hand, computationally they were found at 292 and 318 nm respectively. A small variation was observed because a different phase (gas phase) was used in the theoretical calculation. A peak was observed at 276 nm that might be due to the shifting of electrons from non-bonding orbital to pi antibonding orbital (n—π*) transition [15]. This peak was identified in the quantum chemical spectrum at 356 nm (Table 2). The crucial contributions of the HOMO and LUMO transitions in the gas phase were as follows: HOMO to LUMO transition accounted for 85 % at a wavelength of 356 nm, H-1 to LUMO contributed 82 % at 292 nm, H-4 to LUMO contributed 12 %, H-3 to LUMO contributed 58 %, and H-2 to LUMO contributed 22 % at a wavelength of 318 nm [7,20].

3.3. NMR spectra

The experimental spectrum exhibited a singlet peak at 9.28 ppm owing to the presence of azomethine linkage (-CH═N-) which assures the Schiff base formation (Fig. 1) [27]. A peak for one proton was noticed at 5.99 ppm that referred to isoxazole proton [5,11].

The protons of methyl group attached to isoxazole ring appeared at 2.30 ppm experimentally [27] (Table 3). The azomethine (CH═N), isoxazole, and $–CH_3$ signals were theoretically obtained at 9.55, 6.19, and 2.39 ppm, respectively. A singlet peak was also occurred at 11.28 ppm in the spectrum which attributed to the proton of $–SO_2NH$- moiety [4,28]. This proton signal was theoretically observed at 11.37 ppm. The protons signals for pyridine ring and N-phenyl ring were observed in the range of 8.0–8.20, and 7.48–7.80

Table 1
Characteristics vibrational bands of the studied compound.

Band	Computational (cm^{-1})		Experimental (cm^{-1})
	Unscaled	Scaled[a]	
υ(N–H)	3550	3413	3225
υ(C═N)	1703	1637	1605
υ(SO_2)assym	1320	1269	1304
υ(SO_2)*sym*	1125	1081	1112
υ(C–O)	1300	1250	1240
υ(S–N)	932	896	860

[a] Scaling factor for B3LYP/6-311+G(d, p) is 0.9614.

Table 2
Electronic transitions of the studied compound.

Computational				Experimental	
Wavelength (nm)	Osc. Strength	Symmetry	Major contribution	Wavelength (nm)	Transition
356	0.2423	Singlet-A	HOMO- > LUMO (85 %)	276	n—π^*
318	0.0226	Singlet-A	H-4- > LUMO (12 %), H-3- > LUMO (58 %), H-2- > LUMO (22 %)	256	π—π^*
292	0.0325	Singlet-A	H-1- > LUMO (82 %)	228	π—π^*

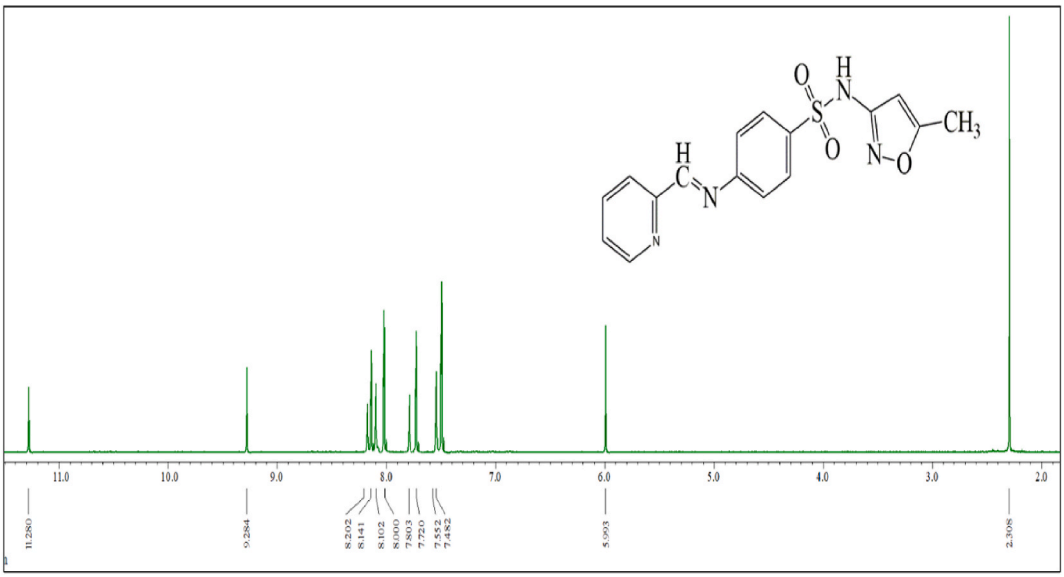

Fig. 1. ^{1}H NMR spectrum of the compound.

ppm [22], respectively, contrariwise they appeared in the range of 7.66–8.99, and 7.31–8.12 ppm, computationally.

3.4. Frontier molecular orbitals analysis (FMO)

The highest occupied molecular orbitals (HOMO) and the lowest unoccupied molecular orbitals (LUMO) are the fraction of the total orbitals that take part in the reactions and significantly represent the reactive cites of a molecule [24,29,30]. The electron donation and acceptation phenomena are governed by the HOMO and LUMO, respectively [31–33]. The FMO analysis ascertains the reactivity of the investigated compounds [34–37]. The biological activity depends on energies of HOMO and LUMO, chemical softness, electrophilicity, as well as maximum charge transfer index descriptors. Higher value of the maximum charge transfer index indicates the greater bioactivity of the molecules. The biological responsiveness increases with decreasing electrophilicity index and chemical softness [38]. The chemical reactivity strongly relies on the HOMO-LUMO energy gap, and the reactivity increases with a lower energy gap. The HOMO energy is equivalent to ionization potential whereas the LUMO energy is directly resembled to electron affinity in accordance with Koopmans theorem [39]. Molecules with lower energy gap are required less amount of energy for excitation and are categorized as chemically soft molecules. Chemically soft molecules are highly bio-active [40]. Various chemical activity descriptors are listed in Table 4. The studied molecule showed a lower energy gap of 4.22 eV, as well as electrophilicity and chemical softness values of 5.30 and 0.24, respectively. These characteristics indicate high reactivity, biological responsiveness, and polarizability of this molecule [6, 41–44].

Table 3
Characteristics ^{1}H NMR data of the studied compound.

Band	Computational (ppm)	Experimental (ppm)
3H, –CH_3	2.39	2.30
1H, isoxazole	6.19	5.99
4H, N-Ph ring	7.31–8.12	7.48–7.80
4H, pyridine ring	7.66–8.99	8.00–8.25
CH═N	9.55	9.28
1H, SO_2NH	11.37	11.28

The HOMOs within the studied compound are observed in pyridine ring and benzene ring, azomethine group, oxygen and nitrogen atoms of sulfonamide group as well as oxazole ring (Fig. 2). While the LUMOs are present in the oxygen and nitrogen atoms of sulfonamide group, azomethine group, pyridine ring, and benzene ring of the sulfamethoxazole part. Additionally, a density of states (DOS) spectrum was generated (Fig. 2). The energy gap resulting from the DOS analysis was 4.20 eV, which closely matches the energy gap obtained from the HOMO-LUMO calculation.

3.5. Molecular electrostatic potential (MEP)

The MEP serves as a quantum computational tool that maps the charge distribution within a molecule, providing insights into its chemical reactivity [33,45]. The nucleophilic, electrophilic, and neutral zones are indicated via blue, red, and green color shades, respectively [46]. The MEP surfaces are plotted in range of −15.95 to 15.95 kJ/mol (-6.075×10^{-3}–6.075×10^{-3} au) (Fig. 3).

The distribution of charge across the surface of molecule provides extensive information about the responsiveness (how it reacts and interacts with other incoming molecules) [38,39]. In this context, higher negative values of MEP delineates the attraction of hydrogen ion/lighter cation in the red zones whereby the electron density is more concentrated in the molecular surface. While, positive values of MEP signifies the repulsive force toward protons/lighter cations in the blue zones with lower concentration of electron density [39,40]. In the studied Schiff base compound the negative zones are situated on the nitrogen atoms of the azomethine part and pyridine ring, oxygen and nitrogen atoms of sulfonamide group and oxazole ring, and on the benzene ring. Hence, these atoms and sites are more likely to affect via electrophilic attack and responsive to form bonds i.e., coordination bond or hydrogen bond. While, the positive zones of the compound are allocated along the hydrogen atoms of the benzene and pyridine rings, carbon atoms of pyridine ring, and on the methyl group of the oxazole portion. The atoms or groups present in the blue zones are prone to nucleophilic attack and able to take part in the hydrophobic interaction.

3.6. ADMET properties and drug likeness

The term ADMET stands for absorption, distribution, metabolism, excretion, and toxicity [2,47]. Drug likeness study reveals the information about the eligibility of molecules to be a drug candidate. The pharmacokinetics properties of the discussed compound was evaluated with the help of ADMETlab 2.0 (https://admetmesh.scbdd.com/service/evaluation/cal) and SwissADME (http://www.swissadme.ch/) bioinformatics web tools and listed in Table 5. Lipinski's rule states that a compound is likely to have adequate absorption and permeability to be an oral drug if it meets the following criteria: molecular weight is $\leq$ 500, n-octanol/water distribution coefficient (LogP) $\leq$5, hydrogen bond donors $\leq$5, and hydrogen bond acceptors $\leq$10. The studied compound followed Lipinski's rule, suggesting it as a potential orally administered and bioavailable drug candidate [48,49]. The Pfizer rule is met when logP >3 and the topological polar surface area (TPSA) is < 75. The GSK rule is satisfied if MW $\leq$ 400 and logP $\leq$4, while the conditions for meeting the Golden Triangle rule are 200 $\leq$ MW $\leq$ 500 and −2 $\leq$ logD $\leq$5; here, logD represents logP at pH 7.4. The compound successfully adheres to the Pfizer rule, Golden Triangle rule, and GSK rule, indicating its potential as a non-toxic drug candidate with a more favorable ADMET profile. All three of the aforementioned rules are completely satisfied by the studied compound. The Caco-2 permeability index tells about human colon adenocarcinoma cell lines. The Caco-2 permeability condition is that the value must be greater than −5.15, if followed, then it is excellently permeable; otherwise, it is poorly permeable. The studied compound is lied in the excellent one. Madin−Darby Canine Kidney Cells (MDCK) permeability index determines the capability of various chemicals to be incorporated into body and also aids in the assessment of blood-brain-barrier (BBB) permeability. The compound is categorized as excellent one by satisfying the optimum-limit must be greater than 2×10^{-6}. The inhibitory capacity of P-glycoprotein (Pgp) is a membrane protein acts as ATP-binding cassette (ABC) transporter. The permissible limit (0–0.3) to be excellent Pgp inhibitor, and Pgp substrate was successfully followed by the studied molecule and classified as excellent one. The Human oral bioavailability index $F_{20\ \%}$ and $F_{30\ \%}$ values appeared within the excellent category range of 0–0.3. The Human intestinal absorption (HIA) index was found to be in the normal limit of 0 up to 0.3 and therefore, categorized as greatly absorbable. The volume distribution (VD) parameter predicts tissue uptakes.

Table 4
Chemical reactivity descriptors of the compound.

Parameters (Unit)	Value
HOMO energy (eV)	−6.84
LUMO energy (eV)	−2.62
Energy gap (eV)	4.22
Ionization potential (eV)	6.84
Electron affinity (eV)	2.62
Chemical hardness (eV)	2.11
Chemical softness (S) (eV^{-1})	0.24
Chemical potential (eV)	−4.73
Electronegativity (eV)	4.73
Electrophilicity index (eV)	5.30
Electro-donating power (eV)	7.93
Electro-accepting power (eV)	3.20
Net electrophilicity (eV)	11.13
Maximum charge transfer index (eV)	2.24

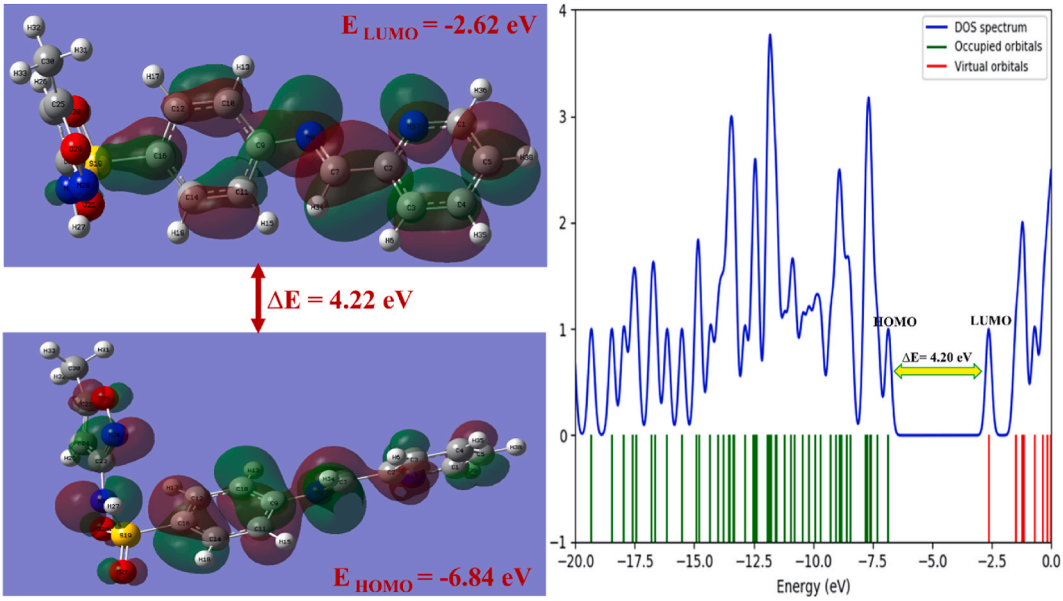

Fig. 2. HOMO-LUMO energies, and DOS spectrum of the compound.

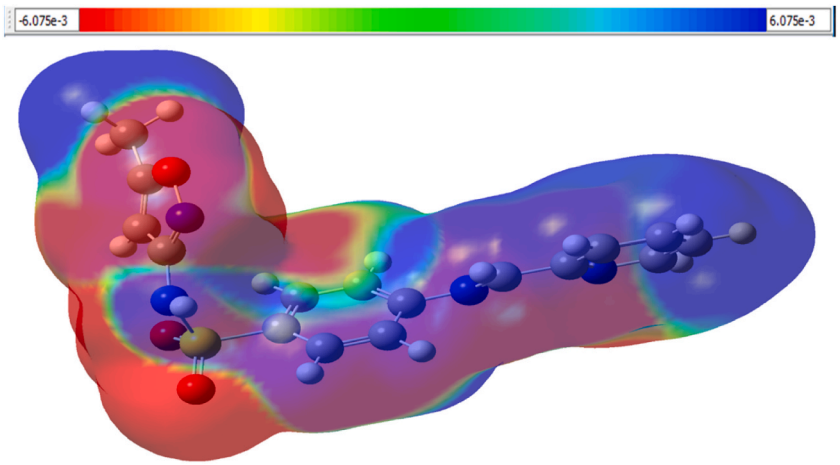

Fig. 3. MEP surface of the studied compound.

Pursuing the normal limits (0.04–20), the molecule is classified as excellent. The ether-a-go-go (hREG) gene plays an important role in heart beating. The hREG blocking is observed within the permissible limit (0–0.3) and the compound is not toxic in terms of hREG blocking. The synthetic accessibility score (SAscore) predicts the ease of preparation of drugs in laboratory. The higher the SAscore, the more difficult it will be in the case of drug preparation. If the score is ≤ 6 and then the drug candidate can be synthesized more easily. The studied compound was scored 2.442. Therefore, it can be easily synthesized in lab. Almost all the toxicity screener parameters such as the hERG blockers, AMES toxicity, rat oral toxicity, skin sensitization, FDAMDD, carcinogenicity, eye corrosion and irritation, and respiratory toxicity lie in the permissible limits. Furthermore, the QED parameter implies that it has attractive drug-likeness character. All absorption parameters including the Caco-2 permeability, MDCK permeability, Pgp-inhibitor and Pgp-substrate, HIA, $F_{20\ \%}$, and $F_{30\ \%}$ are in the accepted range.

3.7. In silico molecular docking

Molecular docking is a computer-based study which provides information about the molecular susceptibility towards specific receptors [50,51]. Pass online is a reliable bioinformatics tool, which suggested that the studied compound can be used as insulysin inhibitor (Fig. 4).). The insulysin inhibition activity of this compound was examined using two target proteins (PDB ID: 3E4A and 3OFI), which were also used in previous research works to evaluate insulysin inhibition activity [52,53]. Both proteins were cumulated

Table 5
ADMET prediction values of the studied compound.

Parameters	Observed value	Parameters	Observed value	Parameters	Observed value
Hydrogen Bond Donor	1	Pgp-substrate	0.001	Rat Oral Acute Toxicity	0.096
Hydrogen Bond Acceptor	7	Pgp-inhibitor	0.014	FDAMDD	0.456
Molecular Mass	342.08	Caco2 permeability	−4.591	AMES Toxicity	0.012
Polar Surface Area	97.45	MDCK permeability	1.3e-05	Carcino-gencity	0.418
Water solubility	−3.508	HIA	0.004	Respiratory Toxicity	0.101
Rotatable Bonds	5	$F_{20\ \%}$	0.003	Eye Corrosion	0.003
LogP	2.889	$F_{30\ \%}$	0.022	Eye Irritation	0.022
QED	0.719	Golden Triangle	Accepted	hERG Blockers	0.018
SAscrore	2.442	Lipinski Rule	Accepted	IGC_{50}	3.893
Skin Sensitization	0.176	Pfizer Rule	Accepted	$LC_{50}FM$	4.229
VDss (human)	0.422	GSK Rule	Accepted	$LC_{50}DM$	4.782

from the protein database (https://www.rcsb.org/structure) [52,54]. Several softwares including LigPlot + v.2.2.8, Autodock_vina_1_1_2, AutoDockTools-1.5.6, and PyMOL-2.5.7 were utilized to perform the docking study [55–58].

The binding pattern of the studied molecule with 3E4A protein reflected that one of the –SO_2- oxygen atoms binds to amino acid Gln111, oxygen atom of the oxazole ring binds to Tyr831, and the azomethine nitrogen binds to Ser128 amino acid through hydrogen bonding with bond distances of 284, 275, and 281 p.m., respectively (Fig. 5(a)).

While the nitrogen atom of pyridine ring, and other ring carbon and hydrogen atoms of the Schiff base bind to amino acids Arg824, Asn139, Ser138, Glu817, Ser132, Phe115, Ala140, and His112 via hydrophobic interaction. The binding modes of the studied compound with 3OFI protein demonstrated that the oxygen atom of the oxazole part binds to amino acid Ser816, and the sulfonamide nitrogen binds to Gly136 amino acid through hydrogen bonding interaction with bond distances of 312, and 328 p.m., respectively (Fig. 5(b)). Rest of the ring carbon and hydrogen atoms, methyl group of the discussed compound bind to amino acids Gln111, Asn139, Ser137, Glu 817, Ser132, Ser128, Leu131, Ser138, Phe115, and His112 through the hydrophobic interaction. A known reference compound ML345 [53] (PubChem-CID: 57390068) was selected, which is used for the comparison of insulysin inhibition capacity with unknown drug candidate. The binding modes of the reference compound (ML345) with 3E4A and 3OFI were visualized in Fig. 6(a) and (b). The binding energies for this reference compound were found to be −8.3 and −8.9 kcal/mol for 3E4A and 3OFI, respectively. Moreover, 6bK (3R,6S,9S,12E,16S)-9-(4-Aminobutyl)-3-[(4-benzoylphenyl)methyl]-6-(cyclohexylmethyl)-2,5,8,11,14-pentaoxo-1,4,7,10,15-pentaazacycloeicos-12-ene-16-carboxamide) is a potential insulin degrading enzyme (IDE) inhibitor used as a standard candidate for in vivo studies [59,60]. To compare the inhibition activity of the query compound with that of 6bK, we have performed in silico docking with the same target proteins (3E4A and 3OFI). The resulting binding energies for 6bK were −10.2 kcal/mol for 3E4A and −9.8 kcal/mol for 3OFI, respectively. On the contrary, the binding energies of the studied compound with the target proteins 3E4A and 3OFI were −9.1 kcal/mol and −8.2 kcal/mol, respectively. Binding energies of the studied compound and standard known compounds are fairly consistent. Therefore, the studied compound has good insulysin inhibition capacity.

3.8. Electron localization function (ELF)/Localized orbital locator (LOL)

The colored graphs with counter lines showed the strong covalent interactions within the compound. This demonstrates the delocalization and localization of electrons and orbital localization, are termed ELF and LOL, respectively [61,62]. The Multiwfn 3.8 program [18] was used to create the wave-functional plots. The higher values of ELF are centered within 0.850–1.000 (red shaded), which indicates that the higher localized electrons are expected to lie in the hydrogen atoms (Fig. 7(a)). This indicates the existence of covalent bonds or lone pair electrons in the compound. The delocalized electrons with lower ELF values lie in the carbon and sulfur atoms (blue shaded) of the studied molecule. The LOL color graph depicts the extent of orbital localization at specific atoms of a

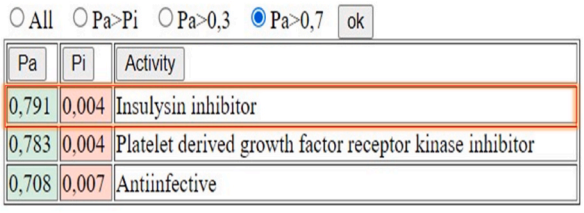

Fig. 4. Prediction result of the compound.

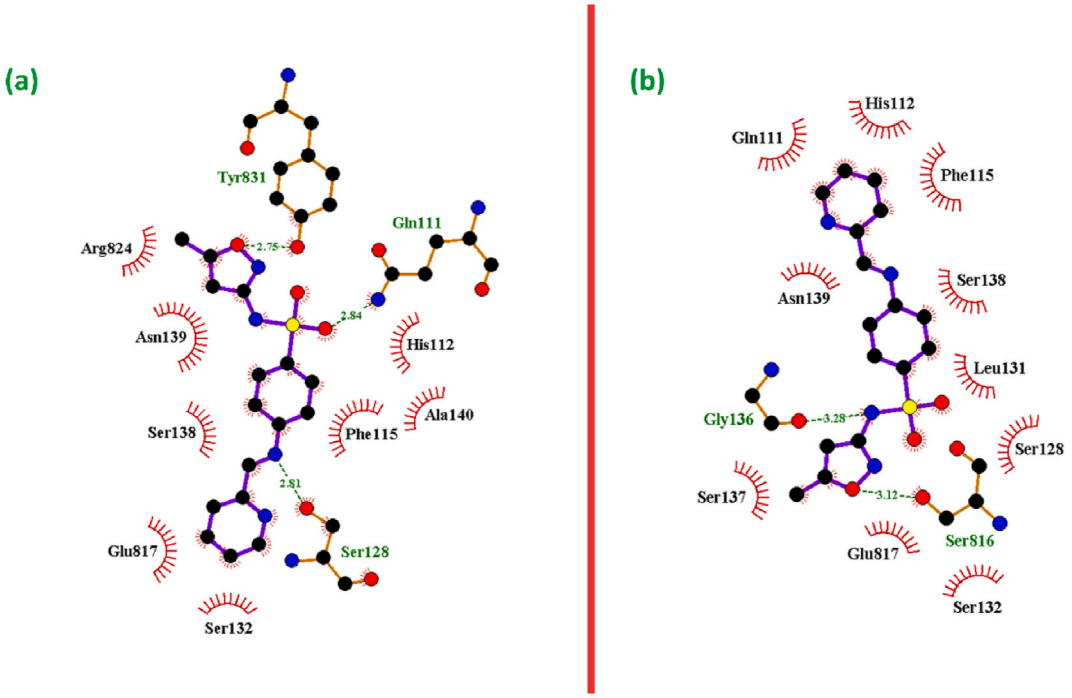

Fig. 5. The binding pattern of the compound with (a) 3E4A and (b) 3OFI.

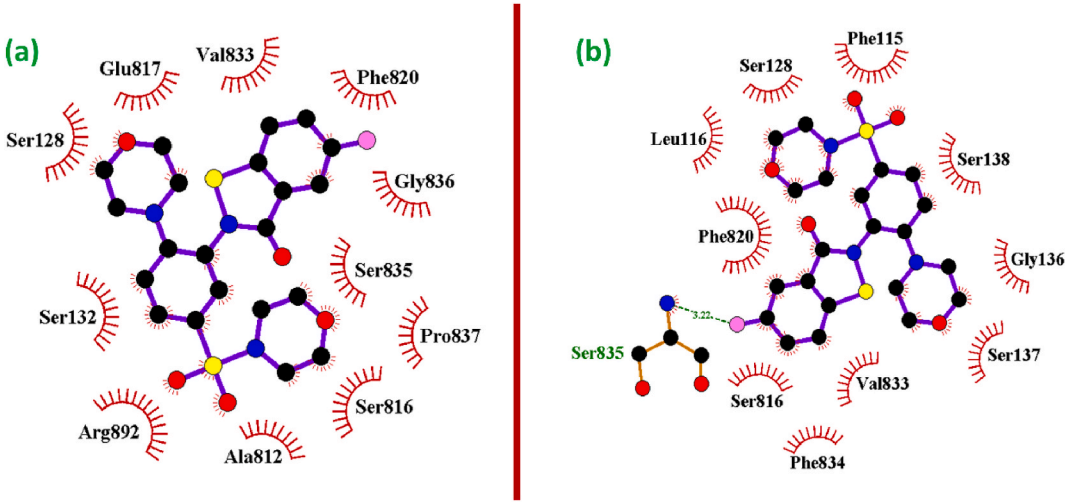

Fig. 6. The binding pattern of ML345 with (a) 3E4A and (b) 3OFI.

molecule, which is plotted in the range of 0.000–0.800 Bohr (Fig. 7(b)). The lower LOL values represented by the blue gradient indicate the weakest orbital delocalization sites, whereas the red gradient with higher values indicates the strongest delocalization. Both ELF and LOL studies give meaningful information about electron placement and bonding natures in query molecules [61]. In the LOL graph C2, C5, C16, C25, and S19 atoms are in the blue zones. The red circle was observed at H38 atom of the molecule (Fig. 7(b)). Both graphs follow Pauli's exclusion principle and the kinetic energy factor [62–64]. The (-N═CH-) bond present in the query compound has significant covalent character and lies in the higher electron concentration zone. The hydrogen atoms of the pyridine ring and azomethine linkage appear white in the central area, indicating that the electron density exceeds the upper range (0.8) in the LOL counter map. This demonstrates the adequate electron delocalization on those atoms, leading to the bio-responsiveness of the studied molecule.

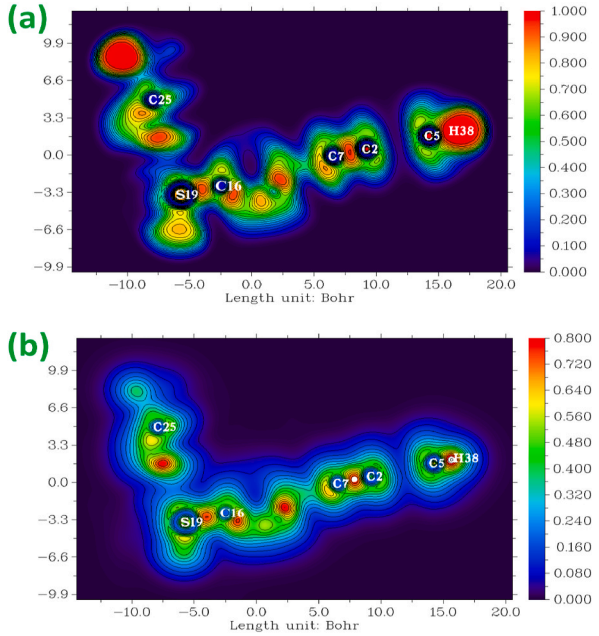

Fig. 7. The wavefunctional map of the studied molecule, (a) ELF and (b) LOL.

3.9. Reduced density gradient (RDG)

The RDG is a time-demanding dimensionless quantity that is used to delineate non-covalent interactions within a molecule [61,65]. The electron density, ρ(r), and the first derivative of it, ∇ρ(r), are employed to evaluate the RDG, which provides detailed insights into the disorderness of electron distribution homogeneity [61,66]. This wavefunctional graph is the plot of RDG vs sign(λ_2)ρ, which dictates the weak interactions present in a molecular system. The higher positive RDG values (red gradient) responsible for the repulsion phenomena, including steric hindrance. The values near to zero (green gradient) are the weaker interaction zones like van der Waals force. The lower negative values (blue gradient) lie in the strongest attraction zones viz. hydrogen-bonds and halogen-bonds in the molecule under study [67]. In the cube image of the compound, steric effect zones are located on the pyridine, aromatic, and oxazole rings, denoted by red plates (Fig. 8). Additionally, weak van der Waals interaction sites are situated around the sulfonamide and azomethine moieties, represented by green gradient plates.

3.10. Natural bond orbital analysis

The natural bond orbital (NBO) analysis was utilized to find out the conjugative interaction, hyper-conjugative interaction,

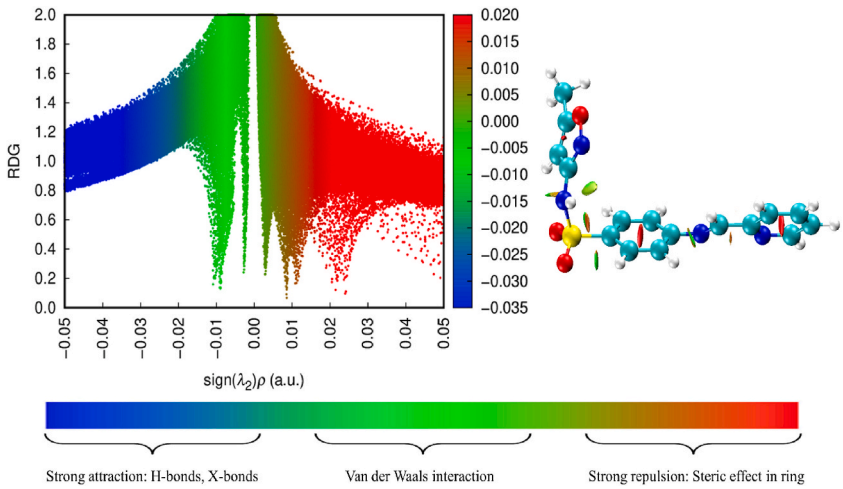

Fig. 8. The RDG map and cube image of the studied molecule.

intramolecular and intermolecular hydrogen bond and electron density distribution between bonding and antibonding orbitals in the molecular system [3,68]. The higher stabilizing energy (E2) can promote extensive conjugation throughout the entire molecular system and determine the stability of the system. Therefore, the molecular system experiences a greater degree of delocalization or electron coupling [69]. NBO analysis was carried out using DFT approach with B3LYP/6-311+G(d, p) basic set. The significant donor-acceptor interactions and their energies are listed in Table 6. Based on the NBO findings, this compound possesses 96.29 % Lewis and 2.71 % non-Lewis character. Although various types of interactions were found in NBO analysis but only π— π* and n— π* interactions were seen in experimental UV–Vis spectrum of the studied compound. Therefore, the NBO results indicate that these two transitions strongly correlate with the observed UV–Vis spectrum. The electronic delocalization of n_2O20→σ*C16–S19, n_2O21→σ*C16–S19 and n_1N37→σ*C1–C5, σ*C2–C3 were found to have moderate effect. The electronic delocalization of n_1N8→π*C9–C11, n_1N22→π*C23–N28, and n_2O29→π*C23–N28, π*C24–C25 were found to have strong effect (Table 6). The most significant π—π* interactions for the pyridine ring in the studied molecule were observed as follows: πC1—N37→π*C2–C3, πC1—N37→π*C4–C5, πC2—C3→π*C1–N37, πC2—C3→π*C4–C5, πC2—C3→π*C7–N8, πC4—C5→π*C1–N37, and πC4—C5→π*C2–C3 with maximum stabilization energies of 25.42, 13.68, 16.82, 20.98, 15.34, 25.68 and 18.72 kcal/mol, respectively. The significant π—π* interactions for azomethine linkage were found as follows: πC7—N8→π*C2–C3, and πC7—N8→π*C9–C11 with minimum stabilization energies of 8.28 and 8.68 kcal/mol, respectively. Additionally, some notable π—π* interactions were observed for the benzene ring as follows: πC10—C12→π*C9–C11, πC10—C12→π*C14–C16, πC14—C16→π*C9–C11, πC14—C16→π*C10–C12 and πC24—C25→π*C23–N28 with values of 21.91, 18.41, 15.19, 20.93 and 27.89 kcal/mol, respectively. Ultimately, the obtained energies contribute to maintaining the stability of the molecular system and demonstrate the interaction between heteroatoms and rings through resonance.

3.11. Non-linear optical analysis (NLO)

NLO materials are recently most important to the current researcher, because of their potential applications in various modern technologies, such as telecommunications, optical interconnections and signal processing field [70,71]. Generally, the NLO properties originate in a molecular system due to the presence of delocalization of π-electrons, electron donor and acceptor group. Besides, NLO properties depend on conjugation length, degree of electron delocalization between the two rings, strength of donor and acceptor groups in the molecular system. The magnitude of the molecular first hyperpolarizability, β is directly related to measure the nonlinear optical activity of a material. Basically, the small energy gap between the HOMO and LUMO orbitals and the large magnitude of linear polarizability exhibit a large first hyperpolarizability value. Therefore, optical properties including dipole moment, polarizability and first order hyperpolarizability of the aforesaid compound were determined using B3LYP/6-311G+(d, p) method in gas phase. The net dipole moment (μ_o), polarizability (α_o) and first order hyperpolarizability (β_o) of the compound were calculated using the following equations [72] and tabulated in Table 7. The calculated polarizability (α_o) and first hyperpolarizability (β_o) values were found as atomic units (a.u), which were converted into electrostatic units by using conversion factor 0.1482×10^{-24} and 0.008639×10^{-30} esu for α and β, respectively.

$$\mu_0 = \sqrt{\mu_x^2 + \mu_y^2 + \mu_z^2} \tag{1}$$

$$< \alpha_o > = \frac{1}{3}\left(\alpha_{xx} + \alpha_{yy} + \alpha_{zz}\right) \tag{2}$$

$$\beta_0 = \sqrt{\beta_x^2 + \beta_y^2 + \mu_z^2} \tag{3}$$

Where,

$$\beta_x = \beta_{xxx} + \beta_{xyy} + \beta_{xzz}$$

$$\beta_y = \beta_{yyy} + \beta_{xxy} + \beta_{yzz}$$

$$\beta_z = \beta_{zzz} + \beta_{xxz} + \beta_{yyz}$$

Urea and potassium dihydrogen phosphate (KDP) are well-known non-linear optical standard substances. These are frequently used for the comparison of NLO properties with the investigated materials. To assess the NLO properties of both urea and KDP molecules, we employed the B3LYP/6-311+G(d, p) basis set. The calculated dipole moment, polarizability, and hyperpolarizability values for urea were found to be 4.48, 4.87×10^{-24} and 1.59×10^{-31}, respectively. For KDP, these values were 8.13, 7.65×10^{-24}, and 9.01×10^{-31}. The corresponding values for the query compound were 6.00, 4.03×10^{-24}, and 2.85×10^{-30}. The hyperpolarizability of the query compound is eighteen times greater than that of urea and three times greater than that of KDP. The studied molecule exhibited higher hyperpolarizability values than both urea and KDP, attributed to electron delocalization and resonance within its two rings and the azomethine linkage throughout the molecular skeleton. This result suggests that the studied molecule could serve as an effective candidate for future nonlinear optical (NLO) applications.

Table 6
Selected second-order perturbation energy values in NBO basis of the studied compound.

Donor NBO (i)	Acceptor NBO (j)	E(2), kcal/mol	Donor NBO (i)	Acceptor NBO (j)	E(2), kcal/mol
σC1-C5	σ*C1–N37	1.46	σS19-O20	σ*C14–C16	0.85
	σ*C4–C5	1.46		σ*C16–S19	0.77
σC1-N37	σ*C1–C5	1.61		σ*S19–O20	0.65
	σ*C2–C7	3.50		σ*S19–O21	0.83
	σ*C2–N37	1.14		σ*S19–N22	2.03
πC1-N37	π*C2–C3	25.42	σS19-O21	σ*C12–C16	0.84
	π*C4–C5	13.68		σ*C16–S19	0.71
σC2-C3	σ*C2–C7	1.83		σ*S19–O20	0.84
	σ*C2–N37	2.21		σ*S19–O21	0.61
	σ*C3–C4	2.55		σ*S19–N22	1.99
	σ*C7–N8	1.53		σ*N22–C23	0.86
πC2-C3	π*C1–N37	16.82	σS19-N22	π*C14–C16	0.98
	π*C4–C5	20.98		σ*C16–S19	0.91
	π*C7–N8	15.34		σ*S19–O20	2.62
σC2-C7	σ*C1–N37	3.17		σ*S19–O21	2.75
	σ*C2–C3	1.67		σ*S19–N22	1.73
	σ*C2–N37	1.54		σ*C23–N28	1.37
	σ*C3–C4	2.18		π*C23–N28	2.16
	σ*C7–N8	2.31	σC23-C24	σ*N22–C23	1.54
	σ*N8–C9	4.16		σ*C23–N28	1.50
σC2-N37	σ*C1–N37	0.98	σC23-N28	σ*S19–N22	1.23
	σ*C2–C3	2.50		σ*N22–C23	0.84
	σ*C2–C7	1.27		σ*C23–C24	2.14
σC3-C4	σ*C2–C3	2.75		σ*C25–C30	0.60
	σ*C2–C7	3.20		σ*S19–N22	3.50
	σ*C4–C5	2.62		σ*C24–C25	7.46
σC4-C5	σ*C1–C5	2.17	σC24-C25	σ*N22–C23	6.95
	σ*C3–C4	2.65		σ*C23–C24	2.16
πC4-C5	π*C1–N37	25.68		σ*C25–C30	2.91
	π*C2–C3	18.72	πC24-C25	π*C23–N28	27.89
σC7-N8	σ*C2–C3	1.28		π*C24–C25	11.56
	σ*C2–C7	1.79	σC25-O29	σ*N22–C23	0.94
	σ*N8–C9	1.56		σ*C24–C25	0.63
	σ*C9–C10	2.00	σC25-C30	σ*C23–C24	0.87
πC7-N8	π*C2–C3	8.28		σ*C24–C25	2.96
	π*C9–C11	8.68		σ*N28–O29	2.16
σN8-C9	σ*C2–C7	3.45	σN28-O29	σ*N22–C23	5.63
	σ*C7–N8	1.25		σ*C25–C30	3.12
	σ*C9–C10	1.43	n_1N8	σ*C2–C7	3.26
	σ*C9–C11	1.49		σ*C9–C11	5.52
	σ*C10–C12	1.57		π*C9–C11	18.12
	σ*C11–C14	1.33	n_1O20	σ*C16–S19	0.70
σC9-C10	σ*C7–N8	2.22		σ*S19–O21	1.86
	σ*N8–C9	1.37	n_2O20	σ*C14–C16	0.60
	σ*C9–C11	3.39		σ*C16–S19	16.40
	σ*C10–C12	2.63		σ*S19–O21	3.61
σC9-C11	π*C7–N8	0.84		σ*S19–N22	9.83
	σ*N8–C9	1.29	n_1O21	σ*C16–S19	0.73
	σ*C9–C10	3.55		σ*S19–O20	1.91
	σ*C11–C14	2.96	n_2O21	σ*C12–C16	0.58
πC10-C12	π*C9–C11	21.91		σ*C16–S19	16.77
	π*C14–C16	18.41		σ*S19–O20	3.80
σC11-C14	σ*N8–C9	3.87		σ*S19–N22	9.11
	σ*C9–C11	2.92	n_1N22	σ*C14–C16	0.70
	σ*C14–C16	3.74		σ*C16–S19	6.49
	σ*C16–S19	3.86		σ*S19–O20	2.25
σC12-C16	σ*C10–C12	2.80		σ*S19–O21	1.37
	σ*C14–C16	4.34		σ*S19–N22	0.50
σC14-C16	σ*C11–C14	2.90		σ*C23–C24	0.55
	σ*C12–C16	4.30		σ*C23–N28	3.62
	σ*C24–C25	2.14		π*C23–N28	20.05
	σ*C25–O29	2.00	n_1N28	σ*N22–C23	0.94
	σ*C25–C30	7.46		σ*C23–C24	5.41
	σ*N28–O29	1.37		σ*C25–O29	4.77
πC14-C16	π*C9–C11	15.19	n_1O29	σ*C23–N28	2.45
	π*C10–C12	20.93		σ*C24–C25	3.19
σC16-S19	σ*C10–C12	2.37	n_2O29	π*C23–N28	14.40
	σ*C11–C14	2.53		π*C24–C25	34.21

(*continued on next page*)

Table 6 (*continued*)

Donor NBO (i)	Acceptor NBO (j)	E(2), kcal/mol	Donor NBO (i)	Acceptor NBO (j)	E(2), kcal/mol
	σ*S19–O20	2.46	n_1N37	σ*C1–C5	9.31
	σ*S19–O21	2.37		σ*C2–C3	10.28
	σ*S19–N22	2.68		σ*C2–C7	2.58

Table 7
Non-linear optical data of the studied compound.

Parameter	Value			Parameter	Value		
	Compound	Urea	KDP		Compound	Urea	KDP
μ_x	5.23	0.00	1.37	β_{xxx}	262.90	0.00	14.25
μ_y	2.86	0.00	−8.01	β_{xxy}	79.24	0.00	−10.62
μ_z	0.71	−4.48	0.00	β_{xyy}	2.47	0.00	−6.06
μ_o	6.00	4.48	8.13	β_{yyy}	75.79	0.00	−83.36
α_{xx}	393.43	23.90	54.92	β_{xxz}	54.04	1.67	0.00
α_{xy}	28.18	0.00	1.24	β_{xyz}	27.47	0.00	0.00
α_{yy}	208.19	36.60	64.89	β_{yyz}	−14.99	−1.60	0.00
α_{xz}	15.66	0.00	0.00	β_{xzz}	29.97	0.00	−0.74
α_{yz}	−23.92	0.00	0.00	β_{yzz}	−10.56	0.00	−10.07
α_{zz}	215.01	38.17	35.07	β_{zzz}	−19.38	−18.50	0.00
α_o, au	272.21	32.89	51.63	β_o, au	329.36	18.43	104.32
α_o, esu	4.03×10^{-24}	4.87×10^{-24}	7.65×10^{-24}	β_o, esu	2.85×10^{-30}	1.59×10^{-31}	9.01×10^{-31}

4. Conclusion

In this study, the Schiff base (E)-N-(5-methylisoxazol-3-yl)-4-((pyridin-2-ylmethylene)amino)benzenesulfonamide was synthesized effectively for experimental and quantum chemical characterization, as well as to explore its drug-like properties and nonlinear optical (NLO) properties. The presence of the azomethine linkage in the molecular skeleton of the Schiff base was confirmed through FT-IR, ^{1}H NMR, and computational results. The studied compound is biologically responsive and highly reactive. The Van deer waals interactions, and steric effect present in the studied molecule. This compound closely adheres to various rules, including Lipinski's, Pfizer, Golden Triangle, and GSK rules. Consequently, the studied molecule is considered non-toxic and a promising candidate for oral drug consumption. Findings from in silico molecular docking analysis suggest that this compound could be a potent insulysin inhibitor in the future. Additionally, the prepared molecule shows potential as an organic NLO material in the field of optoelectronics.

Data availability statement

Data will be made available from corresponding author on reasonable request.

CRediT authorship contribution statement

Md Minhazul Abedin: Writing – review & editing, Writing – original draft, Visualization, Software, Formal analysis. **Tarun Kumar Pal:** Writing – review & editing, Visualization, Supervision, Software, Methodology, Investigation, Formal analysis, Data curation, Conceptualization. **Md Chanmiya Sheikh:** Software, Formal analysis. **Md Ashraful Alam:** Supervision, Conceptualization.

Declaration of competing interest

The authors declare that they have no known competing financial interests or personal relationships that could have appeared to influence the work reported in this paper.

Acknowledgement

We would like to thank the research project of Rajshahi University of Engineering & Technology (DRE/7/RUET/574/2022-23; June 29, 2022) for supporting this research.

References

[1] E. Raczuk, B. Dmochowska, J. Samaszko-Fiertek, J. Madaj, Different Schiff bases—structure, importance and classification, Molecules 27 (2022), https://doi.org/10.3390/molecules27030787.

[2] A.S. Hassan, N.M. Morsy, W.M. Aboulthana, A. Ragab, Exploring novel derivatives of isatin-based Schiff bases as multi-target agents: design, synthesis, in vitro biological evaluation, and in silico ADMET analysis with molecular modeling simulations, RSC Adv. 13 (2023) 9281–9303, https://doi.org/10.1039/d3ra00297g.

[3] Shehnaz, W.A. Siddiqui, M.A. Raza, A. Ashraf, M. Ashfaq, M.N. Tahir, S. Niaz, Structure elucidation {single X-ray crystal diffraction studies, Hirshfeld surface analysis, DFT} and antibacterial studies of sulfonamide functionalized Schiff base copper (II) and zinc (II) complexes, J. Mol. Struct. 1295 (2024) 136603, https://doi.org/10.1016/j.molstruc.2023.136603.

[4] A. Kanagavalli, R. Jayachitra, G. Thilagavathi, M. Padmavathy, N. Elangovan, S. Sowrirajan, R. Thomas, Synthesis, structural, spectral, computational, docking and biological activities of Schiff base (E)-4-bromo-2-hydroxybenzylidene) amino)-N-(pyrimidin-2-yl) benzenesulfonamide from 5-bromosalicylaldehyde and sulfadiazine, J. Indian Chem. Soc. 100 (2023) 100823, https://doi.org/10.1016/j.jics.2022.100823.

[5] N. Uludag, New synthesis of some isoxazole derivatives and their antioxidant properties, Russ. J. Org. Chem. 60 (2024) 490–494, https://doi.org/10.1134/S1070428024030175.

[6] R. Jayachitra, M. Padmavathy, A. Kanagavalli, G. Thilagavathi, N. Elangovan, S. Sowrirajan, R. Thomas, Synthesis, computational, experimental antimicrobial activities and theoretical molecular docking studies of (E)-4-((4-hydroxy-3-methoxy-5-nitrobenzylidene) amino)-N-(thiazole-2-yl) benzenesulfonamide, J. Indian Chem. Soc. 100 (2023) 100824, https://doi.org/10.1016/j.jics.2022.100824.

[7] S. Mondal, S.M. Mandal, T.K. Mondal, C. Sinha, Spectroscopic characterization, antimicrobial activity, DFT computation and docking studies of sulfonamide Schiff bases, J. Mol. Struct. 1127 (2017) 557–567, https://doi.org/10.1016/j.molstruc.2016.08.011.

[8] V. Preethi, V.G. Vijukumar, S. Anilaraj, V.G. Vidya, Heliyon Synthesis , characterization , DFT studies and evaluation of the potential anti-tumour activity of nicotinic hydrazide based Schiff base using in vitro and molecular docking techniques, Heliyon 10 (2024) e29689, https://doi.org/10.1016/j.heliyon.2024.e29689.

[9] S. Paul, M.A. Alam, T.K. Pal, M.N. Uddin, M.M. Islam, M.C. Sheikh, Quantum computational, spectroscopic investigation, molecular docking, and in vitro pharmacological studies of sulfonamide Schiff base, J. Mol. Struct. 1262 (2022) 133084, https://doi.org/10.1016/j.molstruc.2022.133084.

[10] E.E. Porchelvi, S. Muthu, Vibrational spectra, molecular structure, natural bond orbital, first order hyperpolarizability, thermodynamic analysis and normal coordinate analysis of Salicylaldehyde p-methylphenylthiosemicarbazone by density functional method, Spectrochim. Acta Part A Mol. Biomol. Spectrosc. 134 (2015) 453–464, https://doi.org/10.1016/j.saa.2014.06.018.

[11] M.M. Heravi, F. Derikvand, A. Haeri, H.A. Oskooie, F.F. Bamoharram, Heteropolyacids as green and reusable catalysts for the synthesis of isoxazole derivatives, Synth. Commun. 38 (2008) 135–140, https://doi.org/10.1080/00397910701651326.

[12] S. Renuga, S. Muthu, Molecular structure, normal coordinate analysis, harmonic vibrational frequencies, NBO, HOMO-LUMO analysis and detonation properties of (S)-2-(2-oxopyrrolidin-1-yl) butanamide by density functional methods, Spectrochim. Acta Part A Mol. Biomol. Spectrosc. 118 (2014) 702–715, https://doi.org/10.1016/j.saa.2013.09.055.

[13] A. Saleem, U. Farooq, S.M. Bukhari, S. Khan, A. Zaidi, T.A. Wani, A.J. Shaikh, R. Sarwar, S. Mahmud, M. Israr, F.A. Khan, S.A. Shahzad, Isoxazole derivatives against carbonic anhydrase: synthesis, molecular docking, MD simulations, and free energy calculations coupled with in vitro studies, ACS Omega 7 (2022) 30359–30368, https://doi.org/10.1021/acsomega.2c03600.

[14] M.A. Mumit, T.K. Pal, M.A. Alam, M.A.A.A. Islam, S. Paul, M.C. Sheikh, DFT studies on vibrational and electronic spectra, HOMO–LUMO, MEP, HOMA, NBO and molecular docking analysis of benzyl-3-N-(2,4,5-trimethoxyphenylmethylene)hydrazinecarbodithioate, J. Mol. Struct. 1220 (2020) 128715, https://doi.org/10.1016/j.molstruc.2020.128715.

[15] S. Paul, M.A. Alam, T.K. Pal, M.N. Uddin, M.M. Islam, M.C. Sheikh, Quantum computational, spectroscopic investigation, molecular docking, and in vitro pharmacological studies of sulfonamide Schiff base, J. Mol. Struct. 1262 (2022) 133084, https://doi.org/10.1016/j.molstruc.2022.133084.

[16] Zaini Miftach, 済無No Title No Title No Title, 2018, pp. 53–54.

[17] GaussView 6.0.16.Pdf, ((n.d.)).

[18] T. Lu, F. Chen, Multiwfn: a multifunctional wavefunction analyzer, J. Comput. Chem. 33 (2012) 580–592, https://doi.org/10.1002/jcc.22885.

[19] Y. Yamada, S. Gohda, K. Abe, T. Togo, N. Shimano, T. Sasaki, H. Tanaka, H. Ono, T. Ohba, S. Kubo, T. Ohkubo, S. Sato, Carbon materials with controlled edge structures, Carbon N. Y. 122 (2017) 694–701, https://doi.org/10.1016/j.carbon.2017.07.012.

[20] D.M. Gil, F.F. Salomón, G.A. Echeverría, O.E. Piro, H. Pérez, A. Ben Altabef, A detailed exploration of intermolecular interactions in 4-(4-dimethylaminobenzylideneamino)-N-(5-methyl-3-isoxazolyl)benzenesulfonamide and related Schiff bases: crystal structure, spectral studies, DFT methods, Pixel energies and Hirshfeld surface analy, Spectrochim. Acta Part A Mol. Biomol. Spectrosc. 185 (2017) 286–297, https://doi.org/10.1016/j.saa.2017.05.066.

[21] J.H. Solanki, S.I. Marjadi, Synthesis and antimicrobial study of some novel Schiff bases and formazans, Der Pharma Chem. 8 (2016) 80–85.

[22] M.M. Naseer, Z.H. Chohan, Erratum: synthesis, characterization and reactivity towards first-row d-transition metals and biological significance of new pyridinyl derived N-substituted sulfonamides (Journal of Applied Organometallic Chemistry (2007)), Appl. Organomet. Chem. 21 (2007) 826, https://doi.org/10.1002/aoc.1299.

[23] M. Tahriri, M. Yousefi, K. Mehrani, M. Tabatabaee, M.D. Ashkezari, Synthesis, characterization and antimicrobial activity of two novel sulfonamide Schiff base compounds, Pharm. Chem. J. 51 (2017) 425–428, https://doi.org/10.1007/s11094-017-1626-z.

[24] K. Vibha, N.C. Prachalith, R. Annoji Reddy, M.N. Ravikantha, J. Thipperudrappa, Computational studies on sulfonamide drug molecules by density functional theory, Chem. Phys. Impact 6 (2023) 100147, https://doi.org/10.1016/j.chphi.2022.100147.

[25] B. Amul, S. Muthu, M. Raja, S. Sevvanthi, Spectral, DFT and molecular docking investigations on Etodolac, J. Mol. Struct. 1195 (2019) 747–761, https://doi.org/10.1016/j.molstruc.2019.06.047.

[26] A.R. Kumar, L. Ilavarasan, G.P.S. Mol, S. Selvaraj, M. Azam, P. Jayaprakash, M. Kesavan, M. Alam, J. Dhanalakshmi, S.I. Al-Resayes, A. Ravi, Spectroscopic (FT-IR, FT-Raman, UV–Vis and NMR) and computational (DFT, MESP, NBO, NCI, LOL, ELF, RDG and QTAIM) profiling of 5-chloro-2-hydroxy-3-methoxybenzaldehyde: a promising antitumor agent, J. Mol. Struct. 1298 (2024) 136974, https://doi.org/10.1016/j.molstruc.2023.136974.

[27] M. Salehi, M. Kubicki, M. Galini, M. Jafari, R.E. Malekshah, Synthesis, characterization and crystal structures of two novel sulfa drug Schiff base ligands derived sulfonamide and molecular docking study, J. Mol. Struct. 1180 (2019) 595–602, https://doi.org/10.1016/j.molstruc.2018.12.002.

[28] H.E. Gaffer, S.A. Mahmoud, M.S. El-Sedik, T. Aysha, M.H. Abdel-Rhman, E. Abdel-latif, Synthesis, molecular modelling, and antibacterial evaluation of new sulfonamide-dyes based pyrrole compounds, Sci. Rep. 14 (2024) 1–17, https://doi.org/10.1038/s41598-024-60908-8.

[29] S. Alyar, T. Şen, Ü.Ö. Özmen, H. Alyar, Ş. Adem, C. Şen, Synthesis, spectroscopic characterizations, enzyme inhibition, molecular docking study and DFT calculations of new Schiff bases of sulfa drugs, J. Mol. Struct. 1185 (2019) 416–424, https://doi.org/10.1016/j.molstruc.2019.03.002.

[30] K. Benbouguerra, N. Chafai, S. Chafaa, Y.I. Touahria, H. Tlidjane, New α-Hydrazinophosphonic acid: synthesis, characterization, DFT study and in silico prediction of its potential inhibition of SARS-CoV-2 main protease, J. Mol. Struct. 1239 (2021) 130480, https://doi.org/10.1016/j.molstruc.2021.130480.

[31] G. Thilagavathi, A. Kanagavalli, R. Jayachitra, M. Padmavathy, N. Elangovan, R. Thomas, Synthesis, structural, computational, electronic spectra, wave function properties and molecular docking studies of (Z)-4-(((5-methylfuran-2-yl)methylene)amino)-N-(thiazol-2-yl)benzenesulfonamide, J. Indian Chem. Soc. 99 (2022) 100786, https://doi.org/10.1016/j.jics.2022.100786.

[32] D.M. Mamand, Electronic structure , Optoelectronic properties. FTIR , CNMR and HNMR Investigation on 4- ((2-hydroxy-3- Benzene Sulfonamide Molecules at Different Concentrations in DMSO Solvent, 2022, pp. 1–2.

[33] A.I. Aljameel, DFT study of 4-acetamido-N-(3-amino-1,2,4-triazol-1-yl) benzene sulfonamide and its potential application as copper corrosion inhibitor, Int. J. Electrochem. Sci. 17 (2022) 220524, https://doi.org/10.20964/2022.05.39.

[34] N. Nehra, R.K. Tittal, V.D. Ghule, 1,2,3-Triazoles of 8-hydroxyquinoline and HBT: synthesis and studies (DNA binding, antimicrobial, molecular docking, ADME, and DFT), ACS Omega 6 (2021) 27089–27100, https://doi.org/10.1021/acsomega.1c03668.

[35] J.S. Singh, M.S. Khan, S. Uddin, A DFT study of vibrational spectra of 5-chlorouracil with molecular structure, HOMO–LUMO, MEPs/ESPs and thermodynamic properties, Polym. Bull. 80 (2023) 3055–3083, https://doi.org/10.1007/s00289-022-04181-7.

[36] D.D. Li, M.L. Greenfield, Chemical compositions of improved model asphalt systems for molecular simulations, Fuel 115 (2014) 347–356, https://doi.org/10.1016/j.fuel.2013.07.012.

[37] K. Merdja, C.K. Bendeddouche, M. Drissi, F.C. Kaouche, N. Medjahed, J.M. Padrón, M. Debdab, M. Rahmouni, E.H. Belarbi, pt, 1–13, https://doi.org/10.22146/ijc.87476, 2023.

[38] M. Maria Julie, T. Prabhu, E. Elamuruguporchelvi, F.B. Asif, S. Muthu, A. Irfan, Structural (monomer and dimer), wavefunctional, NCI analysis in aqueous phase, electronic and excited state properties in different solvent atmosphere of 3-{(E)-[(3,4-dichlorophenyl)imino]methyl} benzene-1,2-diol, J. Mol. Liq. 336 (2021) 116335, https://doi.org/10.1016/j.molliq.2021.116335.

[39] J.K. Ojha, G. Ramesh, B.V. Reddy, Structure, chemical reactivity, NBO, MEP analysis and thermodynamic parameters of pentamethyl benzene using DFT study, Chem. Phys. Impact 7 (2023) 100280, https://doi.org/10.1016/j.chphi.2023.100280.

[40] M. Miar, A. Shiroudi, K. Pourshamsian, A.R. Oliaey, F. Hatamjafari, Theoretical investigations on the HOMO–LUMO gap and global reactivity descriptor studies, natural bond orbital, and nucleus-independent chemical shifts analyses of 3-phenylbenzo[d]thiazole-2(3H)-imine and its para-substituted derivatives: solvent and subs, J. Chem. Res. 45 (2021) 147–158, https://doi.org/10.1177/1747519820932091.

[41] S. Demir, F. Tinmaz, N. Dege, I.O. Ilhan, Vibrational spectroscopic studies, NMR, HOMO-LUMO, NLO and NBO analysis of 1-(2-nitrobenzoyl)-3,5-diphenyl-4,5-dihydro-1H-pyrazole with use X-ray diffractions and DFT calculations, J. Mol. Struct. 1108 (2016) 637–648, https://doi.org/10.1016/j.molstruc.2015.12.057.

[42] Y. Oueslati, S. Kansız, A. Valkonen, T. Sahbani, N. Dege, W. Smirani, Synthesis, crystal structure, DFT calculations, Hirshfeld surface, vibrational and optical properties of a novel hybrid non-centrosymmetric material (C10H15N2)2H2P2O7, J. Mol. Struct. 1196 (2019) 499–507, https://doi.org/10.1016/j.molstruc.2019.06.110.

[43] S. Kanchana, T. Kaviya, P. Rajkumar, M.D. Kumar, N. Elangovan, S. Sowrirajan, Computational investigation of solvent interaction (TD-DFT, MEP, HOMO-LUMO), wavefunction studies and molecular docking studies of 3-(1-(3-(5-((1-methylpiperidin-4-yl)methoxy)pyrimidin-2-yl)benzyl)-6-oxo-1,6-dihydropyridazin-3-yl)benzonitrile, Chem. Phys. Impact 7 (2023) 100263, https://doi.org/10.1016/j.chphi.2023.100263.

[44] Z. Ye, S. Xie, Z. Cao, L. Wang, D. Xu, H. Zhang, J. Matz, P. Dong, H. Fang, J. Shen, M. Ye, High-rate aqueous zinc-organic battery achieved by lowering HOMO/LUMO of organic cathode, Energy Storage Mater. 37 (2021) 378–386, https://doi.org/10.1016/j.ensm.2021.02.022.

[45] K. Arulaabaranam, S. Muthu, G. Mani, A.S. Ben Geoffrey, Speculative assessment, molecular composition, PDOS, topology exploration (ELF, LOL, RDG), ligand-protein interactions, on 5-bromo-3-nitropyridine-2-carbonitrile, Heliyon 7 (2021) e07061, https://doi.org/10.1016/j.heliyon.2021.e07061.

[46] T.K. Pal, M.A. Mumit, J. Hossen, S. Paul, M.A. Alam, M.A.A.A.A. Islam, M.C. Sheikh, Computational and experimental insight into antituberculosis agent, (E)-Benzyl-2-(4-Hydroxy-2-Methoxybenzylidene) hydrazinecarbodithioate: adme analysis, Heliyon 7 (2021) e08209, https://doi.org/10.1016/j.heliyon.2021.e08209.

[47] O.R. Adianingsih, U. Khasanah, K.D. Anandhy, V. Yurina, In silico ADME-T and molecular docking study of phytoconstituents from Tithonia diversifolia (Hemsl.) A. Gray on various targets of diabetic nephropathy, J. Pharm. Pharmacogn. Res. 10 (2022) 571–594, https://doi.org/10.56499/jppres22.1345.10.4.571.

[48] C.A. Lipinski, F. Lombardo, B.W. Dominy, P.J. Feeney, Experimental and computational approaches to estimate solubility and permeability in drug discovery and development settings, Adv. Drug Deliv. Rev. 64 (2012) 4–17, https://doi.org/10.1016/j.addr.2012.09.019.

[49] A. Al Mahmud, T.K. Pal, M. Monirul Islam, M. Masuqul Haque, M. Al-Amin-Al-Azadul Islam, M. Chanmiya Sheikh, R. Miyatake, S. Paul, Experimental and theoretical insights into structural features of methyl (E)-3-(3,4,5-trimethoxybenzylidene)dithiocarbazate with molecular docking and ADMET studies, J. Mol. Struct. 1287 (2023) 135654, https://doi.org/10.1016/j.molstruc.2023.135654.

[50] P. Ramesh, M. Lydia Caroline, S. Muthu, B. Narayana, M. Raja, S. Aayisha, Spectroscopic and DFT studies, structural determination, chemical properties and molecular docking of 1-(3-bromo-2-thienyl)-3-[4-(dimethylamino)-phenyl]prop-2-en-1-one, J. Mol. Struct. 1200 (2020), https://doi.org/10.1016/j.molstruc.2019.127123.

[51] B. Amul, S. Muthu, M. Raja, S. Sevvanthi, Molecular structure, spectroscopic (FT-IR, FT-Raman, NMR, UV-VIS), chemical reactivity and biological examinations of Ketorolac, J. Mol. Struct. 1210 (2020) 128040, https://doi.org/10.1016/j.molstruc.2020.128040.

[52] S. Chigurupati, V.R. Palanimuthu, S. Kanagaraj, S. Sundaravadivelu, V.R. Varadharajula, Green synthesis and in silico characterization of 4-Hydroxy-3-methoxybenzaldehyde Schiff bases for insulysin inhibition – a potential lead for type 2 diabetes mellitus, J. Appl. Pharmaceut. Sci. 11 (2021) 63–71, https://doi.org/10.7324/JAPS.2021.110706.

[53] S. Hameed, T. Muscat, Molecular designing and docking studies on some novel 5-aryl molecular designing and docking studies on some, 3, https://doi.org/10.20959/wjpps20205-16155, 2020.

[54] Y.S. Mary, H.T. Varghese, C.Y. Panicker, T. Thiemann, A.A. Al-Saadi, S.A. Popoola, C. Van Alsenoy, Y. Al Jasem, Molecular conformational analysis, vibrational spectra, NBO, NLO, HOMO-LUMO and molecular docking studies of ethyl 3-(E)-(anthracen-9-yl)prop-2-enoate based on density functional theory calculations, Spectrochim. Acta Part A Mol. Biomol. Spectrosc. 150 (2015) 533–542, https://doi.org/10.1016/j.saa.2015.05.092.

[55] A. Allouche, Software news and updates gabedit — a graphical user interface for computational chemistry softwares, J. Comput. Chem. 32 (2012) 174–182, https://doi.org/10.1002/jcc.

[56] A.L. Roman, B.S. Mark, LigPlot+: multiple ligand-protein interaction diagrams for drug discovery, J. Chem. Inf. Model. 51 (2011) 2778–2786.

[57] J. Eberhardt, D. Santos-Martins, A.F. Tillack, S. Forli, AutoDock vina 1.2.0: new docking methods, expanded force field, and Python bindings, J. Chem. Inf. Model. 61 (2021) 3891–3898, https://doi.org/10.1021/acs.jcim.1c00203.

[58] A. Allouche, Software news and updates gabedit — a graphical user interface for computational chemistry softwares, J. Comput. Chem. 32 (2012) 174–182, https://doi.org/10.1002/jcc.

[59] J.P. Maianti, A. McFedries, Z.H. Foda, R.E. Kleiner, X.Q. Du, M.A. Leissring, W.J. Tang, M.J. Charron, M.A. Seeliger, A. Saghatelian, D.R. Liu, Anti-diabetic activity of insulin-degrading enzyme inhibitors mediated by multiple hormones, Nature 511 (2014) 94–98, https://doi.org/10.1038/nature13297.

[60] G.R. Tundo, G. Grasso, M. Persico, O. Tkachuk, F. Bellia, A. Bocedi, S. Marini, M. Parravano, G. Graziani, C. Fattorusso, D. Sbardella, The insulin-degrading enzyme from structure to allosteric modulation: new perspectives for drug design, Biomolecules 13 (2023), https://doi.org/10.3390/biom13101492.

[61] S.C. Parakkal, R. Datta, S. Muthu, A. Irfan, A. Jeelani, Computational investigation into structural, topological, electronic properties, and biological evaluation of spiro[1H-indole-3,2′-3H-1,3-benzothiazole]-2-one, J. Mol. Liq. 359 (2022) 119234, https://doi.org/10.1016/j.molliq.2022.119234.

[62] S. Liu, C. Rong, T. Lu, H. Hu, Identifying strong covalent interactions with Pauli energy, J. Phys. Chem. A 122 (2018) 3087–3095, https://doi.org/10.1021/acs.jpca.8b00521.

[63] M. Khodiev, U. Holikulov, A. Jumabaev, N. Issaoui, L. Nikolay Lvovich, O.M. Al-Dossary, L.G. Bousiakoug, Solvent effect on the self-association of the 1,2,4-triazole: a DFT study, J. Mol. Liq. 382 (2023) 121960, https://doi.org/10.1016/j.molliq.2023.121960.

[64] A. Irfan, M. Hussien, A.R. Chaudhry, M.A. Qayyum, A.G. Al-Sehemi, S. Selvakumari, S. Muthu, Effect of solvent role in electronic properties, band gap, electron injection barrier, charge transport nature, topology studies (ELF, LOL, RDG), and optical properties of azoles for multifunctional applications, J. Mol. Liq. 390 (2023) 122956, https://doi.org/10.1016/j.molliq.2023.122956.

[65] J.N.C. Mishma, V.B. Jothy, A. Irfan, B. Narayana, S. Muthu, Role of solvents in molecular level interaction, reactivity and spectral characterisation of 2-Amino-3-(((E)-4-(dimethylamino)benzylidene)amino) maleonitrile: anti depressant agent, J. Mol. Liq. 389 (2023) 122937, https://doi.org/10.1016/j.molliq.2023.122937.

[66] S. Selvakumari, S. Kadaikunnan, G. Abbas, S. Muthu, Computational study of electronic excitations properties in solvents, molecular interaction energies, topological and biological properties of Ethyl 6-bromoimidazo[1,2-a]pyridine-2-carboxylate, Comput. Theor. Chem. 1231 (2023) 114401, https://doi.org/10.1016/j.comptc.2023.114401.

[67] V. Rajmohan, S. Deepa, S. Asha, S.V. Priya, A. Sagaama, M. Raja, Synthesis, solvation effects, spectroscopic, chemical reactivity, topological analysis and biological evaluation of 4-chloro-N-(2, 6-dichlorobenzylidene) benzohydrazide, J. Mol. Liq. 390 (2023) 122955, https://doi.org/10.1016/j.molliq.2023.122955.

[68] N. Elangovan, S.Y. Alomar, S. Sowrirajan, B. Rajeswari, A. Nawaz, A.N. Kalanthoden, Photoluminescence property and solvation studies on (E)-N-(pyrimidin-2yl)-4-((3,4,5-trimethoxy benzylidede) amino) benzene sulfonamide; Synthesis, structural, topological analysis, antimicrobial activity and molecular docking studies, Inorg. Chem. Commun. 155 (2023) 111019, https://doi.org/10.1016/j.inoche.2023.111019.

[69] R. Jayachitra, M. Padmavathy, A. Kanagavalli, G. Thilagavathi, N. Elangovan, S. Sowrirajan, R. Thomas, Synthesis, computational, experimental antimicrobial activities and theoretical molecular docking studies of (E)-4-((4-hydroxy-3-methoxy-5-nitrobenzylidene) amino)-N-(thiazole-2-yl) benzenesulfonamide, J. Indian Chem. Soc. 100 (2023) 100824, https://doi.org/10.1016/j.jics.2022.100824.

[70] S. Selvakumari, K. Murthy Potla, D. Shanthi, A. Irfan, S. Muthu, Solvent effect on molecular, electronic parameters, topological analysis and Fukui function evaluation with biological studies of imidazo [1, 2-a] pyridine-8-carboxylic acid, J. Mol. Liq. 382 (2023) 121863, https://doi.org/10.1016/j.molliq.2023.121863.
[71] M. Vimala, S.S. Mary, A. Irfan, S. Muthu, Solvent role in molecular structure, thermodynamic quantities, reactions and electronic transitions (TDDFT) on 2-[piperidin-1-yl] phenol, J. Mol. Liq. 375 (2023) 121313, https://doi.org/10.1016/j.molliq.2023.121313.
[72] P. Rawat, R.N. Singh, Synthesis, spectral analysis and study of antimicrobial activity of 2,5-diformyl-1H-pyrrole bis(methan-1-yl-1-ylidene)dimalonohydrazone, Arab. J. Chem. 12 (2019) 1219–1233, https://doi.org/10.1016/j.arabjc.2014.10.050.